Fall 8-4-2004

BASS Code Development

Scott Sawyer
The University of Akron, Main Campus, ssawyer@uakron.edu

Final Report – BASS Code Development

Scott Sawyer
Mechanical Engineering
University of Akron
Akron, OH 44325
ssawyer@uakron.edu

Version: August 4, 2004

EXECUTIVE SUMMARY

The BASS computational aeroacoustic code solves the fully nonlinear Euler equations in the time domain in two-dimensions. The acoustic response of the stator is determined simultaneously for the first three harmonics of the convected vortical gust of the rotor. The spatial mode generation, propagation and decay characteristics are predicted by assuming the acoustic field away from the stator can be represented as a uniform flow with small harmonic perturbations superimposed. The computed field is then decomposed using a joint temporal-spatial transform to determine the wave amplitudes as a function of rotor harmonic and spatial mode order. This report details the following technical aspects of the computations and analysis.

- the BASS computational technique
- the application of periodic time shifted boundary conditions
- the linear theory aspects unique to rotor-stator interactions
- the joint spatial-temporal transform

The computational results presented herein are twofold. In each case, the acoustic response of the stator is determined simultaneously for the first three harmonics of the convected vortical gust of the rotor. The fan under consideration here like modern fans is cut-off at BPF, and propagating acoustic waves are only expected at 2BPF and 3BPF. In the first case, the computations showed excellent agreement with linear theory predictions. The frequency and spatial mode order of acoustic field was computed and found consistent with linear theory. Further, the propagation of the generated modes was also correctly predicted. The upstream going waves propagated from the domain without reflection from the inflow boundary. However, reflections from the outflow boundary were noticed. The amplitude of the reflected wave was approximately 5% of the incident wave. The second set of computations were used to determine the influence of steady loading on the generated noise. Toward this end, the acoustic response was determined with three steady loading conditions: design, low-loading, high-loading. The overall trend showed significant ($\backsim$ 10 dB) increases in the generated noise for the highly loaded stator.

Contents

1. INTRODUCTION

Aircraft noise is a significant environmental concern. In fact, NASA under its "Global Civil Aviation pillar" has made a commitment to reduce noise by 10 dB within a decade and 20 dB within the next two decades. Achieving NASA's long-term 20-decibel objective for noise reduction will, in most cases, contain objectionable aircraft noise within the airport boundaries (55 Day Night Level contour), freeing airports of most noise restraints. Aircraft noise has dropped dramatically in the last 30 years with the development of high bypass ratio engines. As the overall noise level has been reduced, fan noise has become more prominent in the engine noise signature. Thus, accurate engine noise predictions will rely heavily on the proper modeling of turbomachinery noise sources.

Discrete-frequency tones are generated by periodic interactions between rotating and non-rotating blade rows. Namely, the fan exit guide vane is subject to the potential field and viscous wake of the fan rotor. The impact of the rotor potential field is mitigated by maximizing the axial spacing between the fan rotor and the exit guide vane. Note that potential flow interactions can become of concern if the axial spacing between blade rows is small or the flow Mach number is high. The viscous wake of the rotor persists over considerable axial distances, and is the primary source of excitation seen by the exit guide vane. The fan exit guide vane operates in an extremely complex flow field generated by highly loaded, arbitrarily shaped airfoils. These complexities change the convection characteristics of the gust and make calculation of the generated noise difficult. The complexity of both the flow and geometry necessitates the solution of the Euler equations on a body-fitted grid.

Rotor wake-stator problems can be solved either in the time or the frequency domain. Both approaches have positive and negative performance and modeling aspects. Frequency domain solvers are typically linearized, depend on an independently determined steady flow, and only solve for one one frequency at a time in either two[1, 2] or three dimensions[3]. Frequency domain solvers typically have lower computational time requirements. By contrast, time domain solvers can easily resolve all frequencies without linearization of the governing equations. Thus, the steady and unsteady flow are determined simultaneously for any amplitude disturbance or response over any number of frequencies. Computational requirements have up to now limited time domain analyses to isolated airfoil problems[4, 5, 6].

The nonlinear Euler equations are solved in the time domain to predict the discrete-frequency noise generated by a rotor wake-stator interaction. The objective of this work is to verify the presence of novel

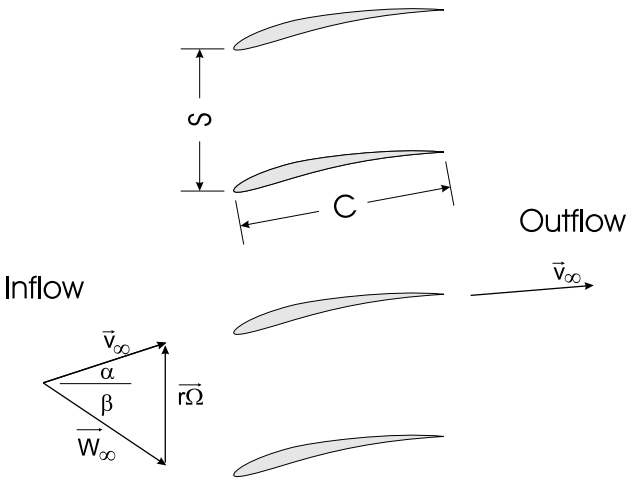

FIG. 1 Two-dimensional cascade representation.

physical phenomena unique to rotor-stator interactions. Assuming the acoustic field can be accurately linearized in the regions upstream and downstream of the stator, the modal structure of the rotor wake-stator generated acoustic waves can be predicted. Then the propagation/decay of the generated waves can also be determined. Thus, comparisons with linear theory are made. It is essential that the linear theory features of the predicted response are well captured. This is accomplished by transforming the computed pressure from a function of position and time $p(x, y, t)$ to a function of axial position, spatial mode and harmonic $P(x, m, n)$ using a joint temporal-spatial transform. It is expected that the rotor wake-stator interaction only produce certain modes, and the propagation/decay of the generated modes conform to linear theory predictions.

2. ROTOR-STATOR INTERACTIONS

Before the linear theory details of the problem are investigated, it is important to delve into some aspects particular to rotor-stator interactions[7]. Consider the interaction of a rotor with N_R blades and a stator with N_S vanes, Fig. 1. The excitation is harmonic in time and periodic in space. The measure of spatial periodicity is the tangential wave number k_y. The tangential wave number is closely related to more commonly known the spatial mode order m which gives the number of periods tangentially around the annulus. The spatial mode order m is related to the tangential wave number $k_y = -\frac{2\pi}{N_S S}m$.

The source of the unsteadiness is the rotor, and the frequency of excitation ω will correspond to the blade passing frequency and its multiples. Further the spatial periodicity of the rotor wakes is determined by the number of rotor blades and the rotor harmonic.

$$\text{rotor excitation:} \qquad \omega = nN_R\Omega \quad \text{and} \quad k_y = -\frac{2\pi}{N_S S}(nN_R) \tag{1}$$

where k_y is the tangential wavenumber, n is the rotor harmonic, S is the stator pitch spacing and Ω is the rotor shaft frequency.

The stator responds at the excitation frequency, and it is expected that the interaction will produce acoustic and vortical waves which satisfy

$$\text{stator response:} \qquad \omega = nN_R\Omega \quad \text{and} \quad k_y = -\frac{2\pi}{N_S S}(nN_R - lN_S) \tag{2}$$

with all values of $l = 0, \pm 1, \pm 2, ...$ expected in the response. Note that an infinite number of spatial modes are generated. However, nearly all of the generated modes will decay exponentially in the duct way from the blade row. Only a relatively small number of these waves will propagate unattenuated in the duct.

In summary, the linear theory analysis can be approached assuming the frequency ω and the tangential wave number k_y are known values (consistent with Eq. 1 or Eq. 2). The acoustic waves generated by this interaction propagate or exponentially decay in the duct upstream and downstream of the stator. The propagation or decay of an acoustic wave can be predicted assuming the acoustic pressure and unsteady velocity are small unsteady perturbations on a uniform mean flow.

3. BASS COMPUTATIONAL TECHNIQUE

The BASS code solves the nonlinear Euler equations in the time domain to determine the acoustic response of a stator to a convected vortical gust. Appropriate boundary conditions must be used at on the stator vane surface and the inflow and outflow boundaries of the domain. The vortical gust of the rotor is specified at the inflow boundary, and the convection of the gust and the resulting response are calculated by the code. The Euler equations in Cartesian coordinates are

$$\frac{\partial \boldsymbol{Q}}{\partial t} + \frac{\partial \boldsymbol{E}}{\partial x} + \frac{\partial \boldsymbol{F}}{\partial y} = 0 \tag{3}$$

where

$$\boldsymbol{Q} = [\tilde{\rho}, \tilde{\rho}\tilde{u}, \tilde{\rho}\tilde{v}, \tilde{E}]$$
$$\boldsymbol{E} = [\tilde{\rho}\tilde{u}, \tilde{\rho}\tilde{u}^2 + \tilde{p}, \tilde{\rho}\tilde{u}\tilde{v}, \tilde{u}(\tilde{E} + \tilde{p})]$$
$$\boldsymbol{F} = [\tilde{\rho}\tilde{v}, \tilde{\rho}\tilde{u}\tilde{v}, \tilde{\rho}\tilde{v}^2 + \tilde{p}, \tilde{v}(\tilde{E} + \tilde{p})]$$

and

$$\tilde{p} = (\gamma - 1)\left(\tilde{E} - \frac{1}{2}\tilde{\rho}(\tilde{u}^2 + \tilde{v}^2)\right)$$

where $\tilde{\rho}$ is the density, $\tilde{u}$ is the velocity in the axial direction, $\tilde{v}$ is the velocity in the tangential direction, $\tilde{p}$ is the pressure, and $\tilde{E}$ is the total energy.

The chain-rule is applied to Eq. 4 to transform the governing equations into curvilinear coordinates.

$$\frac{\partial \boldsymbol{Q}}{\partial \tau} + \left(\xi_x \frac{\partial \boldsymbol{E}}{\partial \xi} + \eta_x \frac{\partial \boldsymbol{E}}{\partial \eta}\right) + \left(\xi_y \frac{\partial \boldsymbol{F}}{\partial \xi} + \eta_y \frac{\partial \boldsymbol{F}}{\partial \eta}\right) = 0 \tag{4}$$

The spatial derivatives of Eq. 4 are then approximated using the prefactored sixth-order compact scheme and explicit boundary stencils of Hixon [8]. Eq. 4 is then integrated in time using a low storage fourth-order nonlinear extension of Hu's 5-6 Low Dispersion and Dissipation Runge-Kutta scheme [9]. Finally, a 10th order explicit filter is used at every stage of the Runge-Kutta solver to dissipate unresolved waves.

On solid boundaries such as the blade surface, the momentum normal to the surface is set to zero at each Runge-Kutta stage ensuring the tangency of the flow with the surface. At the inflow and outflow planes, Giles boundary conditions are used[10].

The computational problem is posed with steady and unsteady boundary conditions. The steady boundary conditions are given so that the nondimensional total pressure, total temperature, inflow absolute flow angle, and exit static to stagnation pressure ratio are specified. These criteria are sufficient to specify the steady flow conditions upstream and downstream of the stator. The unsteady boundary conditions are given to correspond with the convected gust of the rotor at the multiples of the rotor blade pass frequency. The rotor wake is steady in the rotating frame and appears as a velocity deficit in the relative flow direction. In the stationary frame, the rotor wakes are harmonic in time and periodic in the tangential direction. The vortical gust at the inflow plane is given by

$$\vec{u}_g = \sum_{n=1}^{\infty} \{a_n cos(n(k_y y - \omega t) + \phi_n)\} \hat{e}_\beta \tag{5}$$

where $\vec{u}_g = (u_g, v_g)$ is the perturbation velocity, a_n and ϕ_n are the amplitude and phase of the nth harmonic of the rotor wake, ω is the blade passing frequency nondimensionalized by the stator chord and the freestream speed of sound, and $\hat{e}_\beta = (cos\beta, -sin\beta)$ is the unit vector in the direction of the relative flow.

All disturbances such as a convected vortical gust must be introduced at the boundary of the computational domain in a way that is consistent with the governing equations. This is accomplished using a linear theory approximation. Before investigating linear theory, the application of periodic time shifted boundary conditions will be considered.

4. PERIODIC TIME SHIFTED BOUNDARY CONDITIONS

Rotor-stator interaction problems have a natural dependence between time and tangential position due to the periodicity of the rotor and the stator. Each stator passage is excited harmonically by the rotor, and each passage is physically identical to the next. Thus, it is expected that the solution in one passage at a later time to be equal to the solution in an adjacent passage at an earlier time $\tilde{p}(x, y+S, t+\Delta t) = \tilde{p}(x, y, t)$ where $\Delta t = N_R/N_S T$ is the time required for the rotor to move one stator passage and T is the period. That is to say, the solution in passage $n+1$ is expected to lag the solution in passage n, and the solution in passage $n-1$ is expected to lead the solution in passage n by the same Δt. It is impossible to use future events as part of a periodic boundary condition, so a solution that leads by $\Delta t = N_R/N_S T$ is equivalent to one that lags by $\Delta t = T - N_R/N_S T$.

Using this information it is possible to construct periodic time shifted boundary conditions that reduce the computational domain from N_S passages to a single passage. It will be shown how ever that this reduction has an unfortunate side effect. Figure 2 shows (1) the computational domain has been reduced to a single passage allowing solution on a single computational node, (2) only the current time step the solution is required in the passage itself, and (3) the creation of computational buffers that keep a time history of the solution so that the buffer data can be used with the proper time lag. To illustrate, consider a rotor with $N_R = 11$ blades interacting with a stator that has $N_S = 27$ stator vanes. If roughly 2400 time steps are taken per period, the lagging buffer needs to contain about 978 time steps, and the leading buffer needs to contain about 1400 time steps. The storage requirements are not overly onerous.

Now imagine the rotor wake entering the computational domain, it will naturally take some time for the wake to convect into the domain and interact with the stator and reach a periodic solution. Consider the solution to this problem using a parallel cluster, Figure 3. Each node of the cluster is assigned a passage, and the solution in each passage is determined simultaneously. Based on current experience a steady state solution is obtained in roughly 100 to 200 periods. The unattractive aspect in imposing time shifted boundary conditions is the additional 978 to 1400 time steps required for the disturbance to propagate through the computational buffer. This means that 1400 computational steps are taken before the initial disturbance even comes back into the solution. Even more time is required for the solution in the time shifted computational buffers to reach steady state. The estimated time required to reach a periodic solution, based on the size of the larger buffer, is 11 to 16 times longer than the parallel solution. The time shifted computational buffers represent all of the passages of the stator (27) but are split between two buffers, 11 in one and 16 in the other. Due to the dramatic increase solution time and the corresponding availability of suitable parallel computing facilities, periodic boundary conditions were not integrated into the production framework of BASS code.

5. LINEAR THEORY

In present form, the BASS code determines the unsteady aerodynamic and acoustic response to a convected vortical gust that is specified at the inflow boundary of the computational domain. Our endeavor here is to determine a method by which acoustic disturbances may also be included. This is accomplished by assuming the unsteady velocity and the acoustic field are a small perturbation on a uniform mean flow. The linearized Euler equations are homogeneous and have acoustic and vortical wave solutions. This closely follows the work of Smith[11].

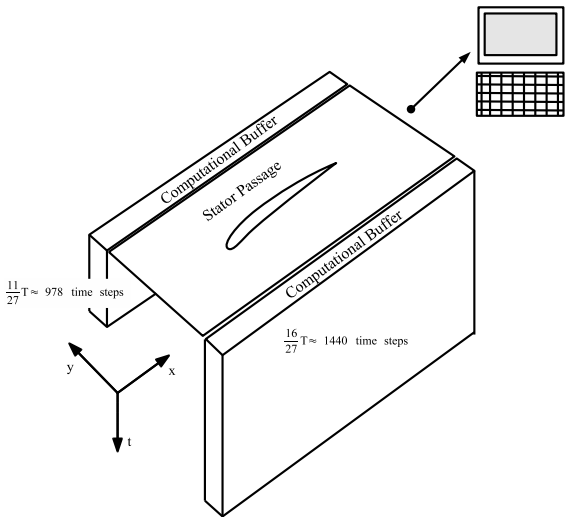

FIG. 2 Periodic boundary conditions – computational data is buffered in time. This allows the calculation of the solution on a single node.

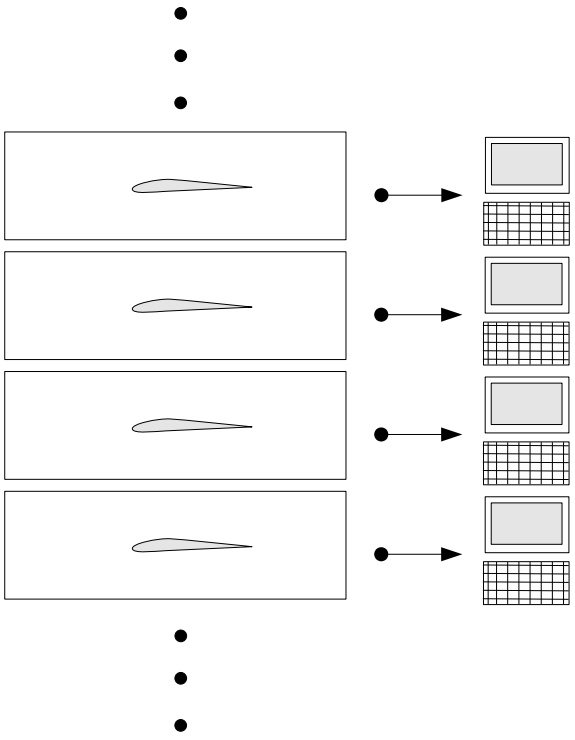

FIG. 3 A multipassage calculation computed on a parallel cluster of computers. No buffering of the computational data is required. All passages of the stator are determined simultaneously.

Away from the stator vane passage, the unsteady velocity and acoustic fields are represented as small perturbations superimposed on a uniform mean flow. Linearizing the flow variables gives

$$\tilde{\rho} = \rho_\infty + \rho$$
$$\tilde{u} = U + u$$
$$\tilde{v} = V + v$$
$$\tilde{p} = p_\infty + p$$

where ρ_∞ is the freestream density, ρ is the perturbation density, $\boldsymbol{v} = (u, v)$ is the perturbation velocity, p is the acoustic pressure, and $\boldsymbol{V} = (U, V)$ is the freestream velocity.

Linearization of the problem in this way will lead to the decomposition of the unsteady acoustic and velocity field into upstream and downstream going acoustic waves and a convected vorticity wave. The linearized Euler equations govern the flow in this region away from the stator.

$$\frac{D\rho}{Dt} + \rho_\infty \nabla \cdot \boldsymbol{v} = 0 \tag{6}$$
$$\rho_\infty \frac{D\boldsymbol{v}}{Dt} + \nabla p = 0 \tag{7}$$

where $\frac{D}{Dt} = \frac{\partial}{\partial t} + (\boldsymbol{V} \cdot \nabla)$. The perturbations in pressure and density are related $p = a_\infty^2 \rho$ where a_∞ is the freestream speed of sound. Assuming a wave type solution gives

$$\begin{Bmatrix} u \\ v \\ p \end{Bmatrix} = \begin{Bmatrix} \bar{u} \\ \bar{v} \\ \bar{p} \end{Bmatrix} e^{i(k_x x + k_y y + \omega t)} \tag{8}$$

where k_x and k_y are the wave numbers in the axial and tangential directions, ω is the frequency of the excitation, and the overbar quantities are the perturbation amplitudes. Substitution of Eq. 8 into Eq. 6 and Eq. 7 gives a homogeneous linear system of equations.

$$\begin{bmatrix} (\omega + Uk_x + Vk_y) & 0 & k_x/\rho_\infty \\ 0 & (\omega + Uk_x + Vk_y) & k_y/\rho_\infty \\ a^2\rho_\infty k_x & a^2\rho_\infty k_y & (\omega + Uk_x + Vk_y) \end{bmatrix} \begin{Bmatrix} \bar{u} \\ \bar{v} \\ \bar{p} \end{Bmatrix} = 0 \tag{9}$$

All nontrivial solutions to these equations must have a determinant equal to zero. In nondimensional terms, the determinant is

$$[M^2(k + k_x cos\alpha + k_y sin\alpha)^2 - (k_x^2 + k_y^2)](k + k_x cos\alpha + k_y sin\alpha) = 0 \tag{10}$$

where the reduced frequency $k = \omega C/|\boldsymbol{V}|$, C is the chord, M is the freestream Mach number, and α is the absolute flow angle. Eq. 10 describes three waves. The first two are acoustic waves which travel upstream and downstream from the cascade, and the third is a vortical wave convected with the mean flow. The axial wavenumber can be determined for a given reduced frequency and a tangential wave number that satisfies rotor-stator periodicity requirements.

5.1. Vorticity Wave Solution

A vorticity wave has an axial wave number that satisfies $(k + k_x cos\alpha + k_y sin\alpha)$. This gives

$$k_{x3} = -\frac{k + k_y sin\alpha}{cos\alpha}$$

where the subscript 3 is used to denote vorticity waves.

The vorticity ξ is determined taking by the curl of the velocity. In two dimensions, this gives

$$\xi = \bar{\xi} e^{i\omega t} = \frac{\partial v}{\partial x} - \frac{\partial u}{\partial y} \tag{11}$$

Substitution of the Eq. 8 into Eq. 11 yields

$$\bar{\xi} = k_{x3}\bar{v}_3 - k_y\bar{u}_3 \tag{12}$$

The continuity equation can be simplified to show

$$k_{x3}\bar{u}_3 + k_y\bar{v}_3 = 0 \tag{13}$$

Solving Eq. 13 for the tangential velocity perturbation $\bar{v}_3$ gives

$$\bar{v}_3 = -\frac{k_{x3}}{k_y}\bar{u}_3 \tag{14}$$

Substituting Eq. 14 into Eq. 12 gives the amplitude of the velocity perturbation $(\bar{u}_3, \bar{v}_3)$ in terms of the amplitude of the vortical wave $\bar{\xi}_3$.

$$\bar{u}_3 = -[k_{x3}^2/k_y + k_y]^{-1}\bar{\xi}_3 \tag{15a}$$

$$\bar{v}_3 = [k_{x3} + k_y^2/k_{x3}]^{-1}\bar{\xi}_3 \tag{15b}$$

The axial momentum equation can be simplified to show

$$\bar{u}_3 = -\frac{k_{x3}}{M(k + k_{x3}cos\alpha + k_y sin\alpha)} \frac{\bar{p}_3}{\rho_\infty a_\infty}$$

The axial wave number k_{x3} ensures that the denominator of this expression is zero. For a bounded axial velocity $\bar{u}_3$, the acoustic perturbation $\bar{p}_3$ associated with the vortical wave must be identically zero $\bar{p}_3 \equiv 0$. Thus, the vortical wave has no acoustic part.

In summary, a vorticity wave is simply convected with the mean flow. The vorticity wave corresponds with a perturbation in velocity and has no acoustic part. Eq. 15 can be used to determine the amplitude of the velocity perturbation given the amplitude of the vorticity wave.

5.2. Acoustic Wave Solutions

Acoustic wave solutions have axial wave numbers that satisfy

$$M^2(k + k_x cos\alpha + k_y sin\alpha)^2 - (k_x^2 + k_y^2) = 0 \tag{16}$$

Eq. 16 is quadratic in the axial wavenumber k_x and two roots can be determined.

$$k_{x1,2} = \frac{M^2 cos\alpha(k + k_y sin\alpha) \pm \sqrt{M^2(k + k_y sin\alpha)^2 - (1 - M^2 cos^2\alpha)k_y^2}}{1 - M^2 cos^2\alpha} \tag{17}$$

where the subscript 1 or 2 is used to denote upstream or downstream going waves, respectively. The propagation/decay characteristic of an acoustic wave is determined by the argument of the square root.

- $M^2(k + k_y sin\alpha)^2 - (1 - M^2 cos^2\alpha)k_y^2 > 0$, there are two real wave numbers which describe waves that propagate upstream and downstream in the duct.
- $M^2(k + k_y sin\alpha)^2 - (1 - M^2 cos^2\alpha)k_y^2 < 0$, there is a complex conjugate pair of wave numbers describing waves which must decay exponentially away from the cascade.

- $M^2(k + k_y sin\alpha)^2 - (1 - M^2 cos^2\alpha)k_y^2 = 0$, there are real repeated wave numbers which describe an acoustic resonance condition.

Acoustic waves which decay in the duct are called "cut-off", and waves which propagate are called "cut-on". An acoustic wave will propagate when the spatial mode order falls in the range $m_1 < m < m_2$ where m_1 and m_2 are given by

$$m_{1,2} = \frac{N_S S}{2\pi} \frac{kM}{1 - M^2} \left[M \sin\alpha \pm \sqrt{1 - M^2 \cos\alpha^2} \right] \tag{18}$$

The axial and tangential momentum equations, Eq. 9, can be used to relate the amplitude of the velocity perturbation with the pressure perturbation.

$$\bar{u}_{1,2} = -\frac{k_{x1,2}}{M(k + k_{x1,2} cos\alpha + k_y sin\alpha)} \frac{\bar{p}_{1,2}}{\rho_\infty a_\infty} \tag{19a}$$

$$\bar{v}_{1,2} = -\frac{k_y}{M(k + k_{x1,2} cos\alpha + k_y sin\alpha)} \frac{\bar{p}_{1,2}}{\rho_\infty a_\infty} \tag{19b}$$

In summary, acoustic waves result in perturbations in pressure, density and velocity, but contain no vortical part. Eq. 19 is used to determine the amplitude of the velocity perturbation given the amplitude of the acoustic wave. The acoustic waves must exist at a multiple of BPF $\omega = nN_R\Omega$ and have a spatial periodicity which satisfies $k_y = -\frac{2\pi}{N_S S}(nN_R - lN_S)$ where l is any integer.

6. JOINT SPATIAL-TEMPORAL TRANSFORM

In a rotor-stator interaction, the response is not only harmonic in time, but also periodic in the tangential direction y, and Fourier transforms in time and space are applied. The acoustic pressure, computed N_t times at position (x, y) over the interval $T = N_t \Delta t$ where Δt is the time between samples, can be decomposed using a joint Fourier transform of the acoustic pressure $p(x, y, t)$. The joint transform gives the acoustic pressure as a function of axial location, frequency and spatial mode order $\bar{p}(x, m, n)$. The joint Fourier transform is

$$\bar{p}(x, m, n) = \frac{2}{NN_t} \sum_{l=0}^{N-1} \sum_{j=0}^{N_t-1} p_{lj}(x)\ e^{-2\pi i(nj/N_t + ml/N)} \tag{20}$$

where $p_{lj}(x)$ is $p(x, y_l, t_j)$, $n = 0, ..., N_t/2$, the frequency $f_n = n/T$, N is the number of points in the tangential direction y, and $-N/2 < m < N/2$ is the spatial mode order. Note that only integer values of m are allowed (corresponding with an integer number of periods around the annulus). Also keeping only positive frequencies implies the rotor and its convected gust are rotating with the rotor shaft in the positive direction.

In summary, the computed acoustic pressure can be decomposed in time and space to determine the amplitude of the acoustic waves as a function of rotor harmonic n, spatial mode order m and axial location x. The behavior of the decomposed acoustic field will then be compared with the behavior of the waves predicted by classical linear theory where only certain spatial modes are generated by the rotor-stator interaction and the propagation or exponential decay of the generated modes can be predicted.

7. COMPUTATIONAL RESULTS

The interaction of a rotor and stator in an annular duct generates acoustic waves at the multiples of the rotor blade pass frequency. The acoustic waves in the annulus are naturally periodic in the circumferential direction. The spatial mode order is the measure of the circumferential periodicity and gives the number of periods over circumference of the annulus. For a rotor and stator with N_R rotor blades and N_S stator vanes it is possible to predict the spatial mode order of the generated waves. Further, the axial propagation, decay or resonance of the generated waves can also be predicted assuming the acoustic waves are a small unsteady

perturbation on the mean flow. The amplitude of the response depends on the frequency of the excitation, the geometry of the stator, and the steady stator loading. Thus, the objectives of the previous research were twofold. First, the linear theory characteristics of the response were used to support the fidelity of the computed solution. Second, the influence of the steady loading on the amplitude of the response was determined.

In each case the same stator was considered, the geometry is a typical of a high performance stator vane row of aircraft engine fan. The stator has $N_S = 27$ vanes and is excited by the wakes of $N_R = 11$ rotor blades. The computational grid for one passage, shown in Fig. 4, contains 9 blocks and 12,700 points per passage. The cascade has a pitch spacing $S/C = 2/3$. Note doubling the grid density changed the response by less than 2%. The mean inflow and outflow conditions at the design condition are given by

$$\text{inflow:} \begin{cases} P_i = 1 \\ T_i = 1 \\ \alpha_i = 36^o \end{cases} \qquad \text{outflow: } p_o/P_i = 0.92 \tag{21}$$

where P_i is the nondimensional stagnation pressure at the inlet, T_i is the nondimensional stagnation temperature at the inlet, α_i is the absolute flow angle at the inlet, and p_o is the nondimensional static pressure at the exit.

The stator is excited by the convected gust of the rotor at the first three multiples of the rotor blade pass frequency. The rotor wake is steady in the rotating frame and appears as a velocity deficit in the relative flow direction. In the stationary frame, the rotor wakes are harmonic in time and periodic in the tangential direction. The vortical gust at the inflow plane is given by

$$\boldsymbol{u_g} = \{a_1 cos[k_y y - \omega t] + a_2 cos[2(k_y y - \omega t) + \phi_2) + a_3 cos[3(k_y y - \omega t) + \phi_3]\}\hat{e}_\beta \tag{22}$$

where $\hat{e}_\beta = (cos\beta, -sin\beta)$ is the unit vector in the direction of the relative flow, the relative flow angle $\beta = 50^o$. For the case under consideration here, the excitation frequency $\omega = 3\pi/4$ and the tangential wave number $k_y = 11\pi/9$. The amplitude of the gust is

$$\begin{aligned} a_1 &= 7 \times 10^{-3} \\ a_2 &= 3 \times 10^{-3} \qquad & \phi_2 &= -7\pi/5 \\ a_3 &= 7 \times 10^{-4} & \phi_3 &= -\pi/2 \end{aligned}$$

7.1. Prediction of Discrete Frequency Noise Generated by a Rotor Wake-Stator Interaction

Fig. 5 shows the acoustic pressure at an instant in time corresponding to the beginning of the period ($t/T = 0$) for a portion of the 27 vane cascade. The tangential periodicity in the solution is evident. The maximum nondimensional acoustic pressure in the computational domain $p_{max} = 0.03$ or 163 dB occurs at the leading edge. Away from the cascade the acoustic pressure is on the order of 122 dB. The time evolution of this field is decomposed using the joint spatial-temporal transform to determine the acoustic pressure as a function of rotor harmonic n, spatial mode order m and axial location in the duct x. The transform is accomplished by saving 64 snapshots over the course of two periods of excitation. A temporal Fourier transform is applied to transform from the time to the frequency domain where only positive frequencies are kept (i.e. $n = 0, 1/2, 1, 3/2, ..., 32$). Response is only expected at $n = 1,\ 2$ and 3. To accomplish the spatial transform rectangular regions are extracted upstream and downstream of the cascade. The acoustic pressure is now known as a function of position (x, y) and harmonic n. The spatial Fourier transform is applied to remove the dependence on y. The computed acoustic field can now be represented as a function of axial position x for a given harmonic n and spatial mode order m, but before showing the computed results the linear theory analysis will be applied to predict (1) the generated spatial modes and (2) the cut-off spatial mode order for propagation/decay of the wave in the duct.

It is expected that the rotor-stator interaction will produce acoustic waves at the frequencies it is excited ($n = 1, 2, 3$) and no others. Fig. 6 shows the time history and the amplitude of the pressure spectrum at

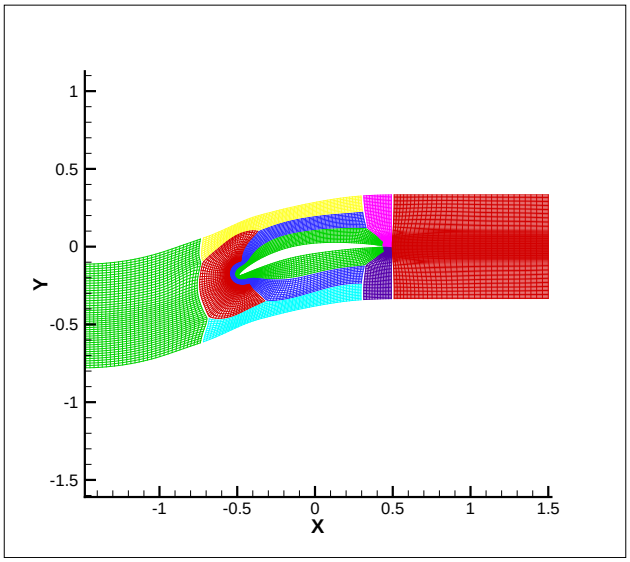

FIG. 4 Computational grid for one of the 27 stator vane passages.

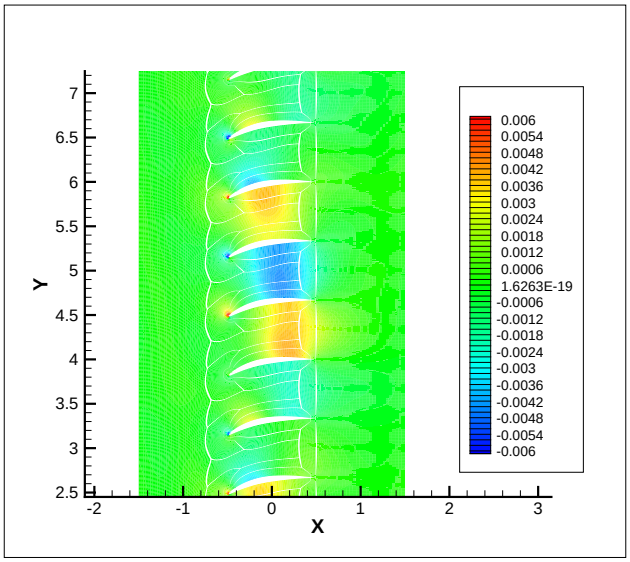

FIG. 5 Instantaneous acoustic pressure at t/T=0.

n	Generated Modes Spatial Mode Order			
1	11	-16	-43	-70
2	22	-5	-32	-59
3	33	6	-21	-48

TABLE 1
Generated acoustic modes.

	Upstream		Downstream	
	Abs flow angle	35.99	Abs flow angle	-0.16
	Mach Number	0.443	Mach Number	0.338
	Reduced Frequency	5.32	Reduced Frequency	6.97
n	m1	m2	m1	m2
1	-10.03	5.65	-7.16	7.18
2	-20.05	11.31	-14.33	14.36
3	-30.08	16.96	-21.49	21.54

TABLE 2
Propagating spatial modes $\mathbf{m_1} < \mathbf{m} < \mathbf{m_2}$.

the inflow plane $(x, y) = (-1.5, 0)$. Clearly, the computed acoustic response is behaving in a linear manner without any evidence of nonharmonic response.

The spatial modes generated at the first three rotor harmonics determined using Eq. 2, $m = nN_R - lN_S$, are shown in Table 1. The computed results now decomposed in time and space are shown at the inflow plane ($x = -1.5$) for all three harmonics, Fig. 7. The computed pressure exists only at the predicted spatial mode orders with no modal "spillover".

Now the range of spatial mode which will propagate in the duct can be determined by application of Eq. 18, Table 2. The change in the mean flow variables upstream and downstream of the cascade changes significantly the range of propagating spatial modes. Note that the acoustic response is "cut-off" at BPF with no propagating waves. At 2BPF, there is one wave $m = -5$ propagating upstream and downstream in the duct. At 3BPF, there are two waves $m = -21$ and 6 propagating in the upstream duct, but only one $m = 6$ propagating in the downstream duct. Note in the downstream duct the wave $m = -21$ at 3BPF is very near the linear theory resonance condition.

Finally, the linear theory analysis gives the ability to examine the axial behavior of the generated modes in the duct. Several things are expected: (1) decaying waves decay exponentially away from the cascade; (2) propagating waves propagate with constant amplitude; and (3) the generated waves exit the domain without reflection from the inflow or outflow boundaries.

The axial wavelengths and wavenumbers of the propagating waves can be analytically predicted using Eq. 10. Here the change in the mean flow variables upstream and downstream of the cascade causes only small changes in the wavelengths of the generated modes, Table 3. Note numerical dispersion in the computed results will cause the computed wavenumbers/wavelengths to differ from these analytically predicted values.

The behavior of the generated modes at each multiple of BPF will be examined in turn. The acoustic response at BPF is shown in Fig. 8. As predicted, the generated waves decay in the direction away from the cascade.

Fig. 9 shows a series of plots related to the propagation or decay of the modes generated at 2BPF in the region upstream of the cascade. Fig. 9(a) shows the amplitude of the generated waves as a function of axial location x. The $m = -5$ mode propagates at nearly constant amplitude ($2.45E-04, 121.3$ dB) while all other generated waves decay in the direction away from the cascade. Fig. 9(b) shows the $m = -5$ mode with the nearly linear phase distribution of an upstream traveling wave. Fig. 9(c) shows the complex amplitude of the $m = -5$ mode. A perfectly propagating upstream going wave would appear on Fig. 9(c) as a circle.

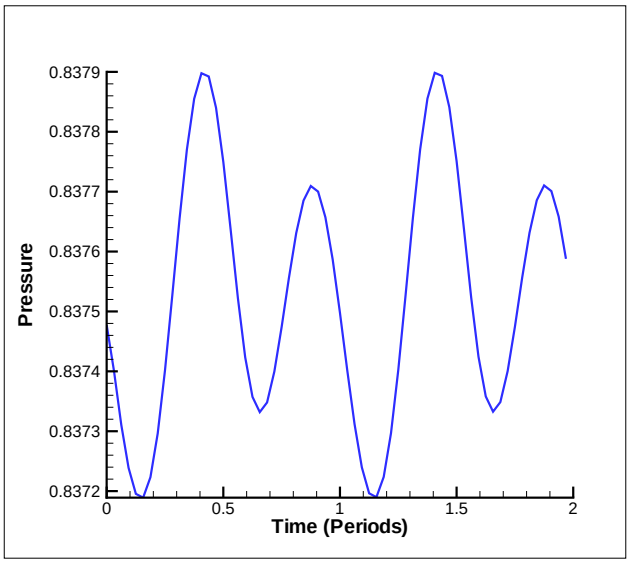

(a) Pressure time history.

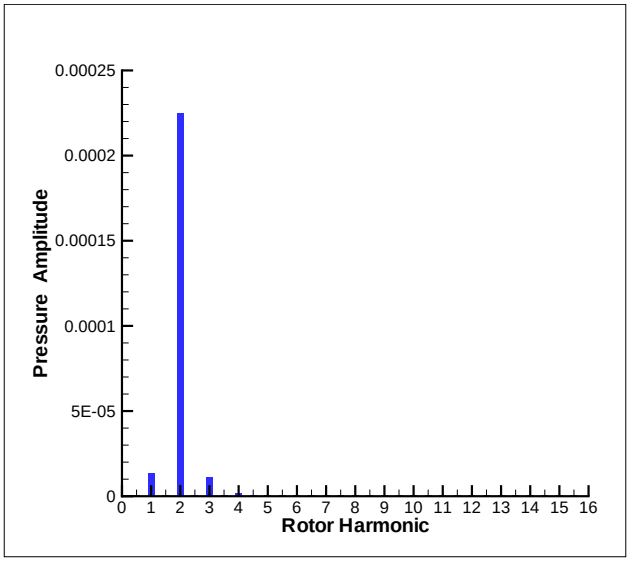

(b) Amplitude of the pressure spectrum.

FIG. 6 Pressure history and spectrum at $(x, y) = (-1.5, 0)$.

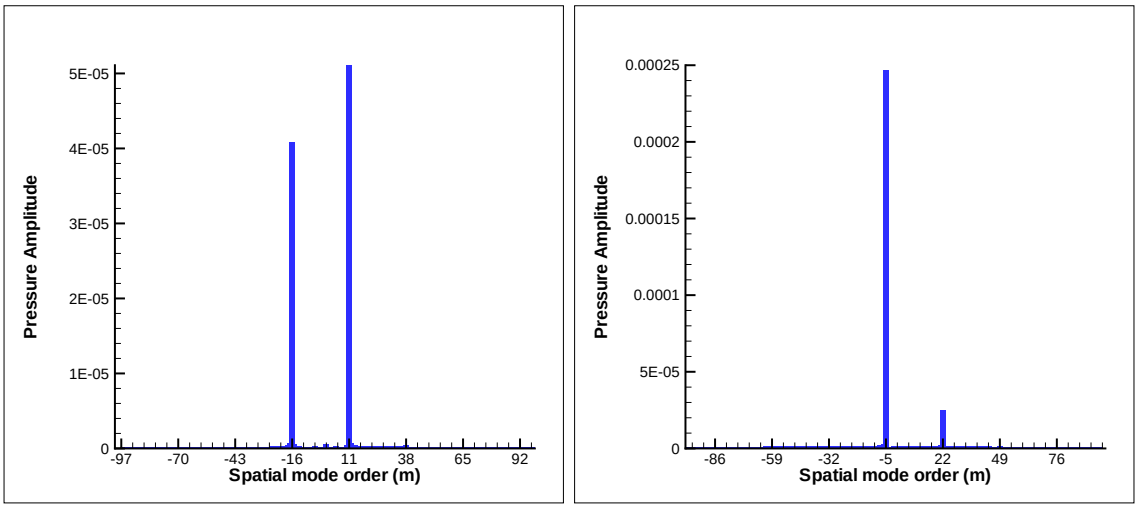

(a) BPF

(b) 2BPF

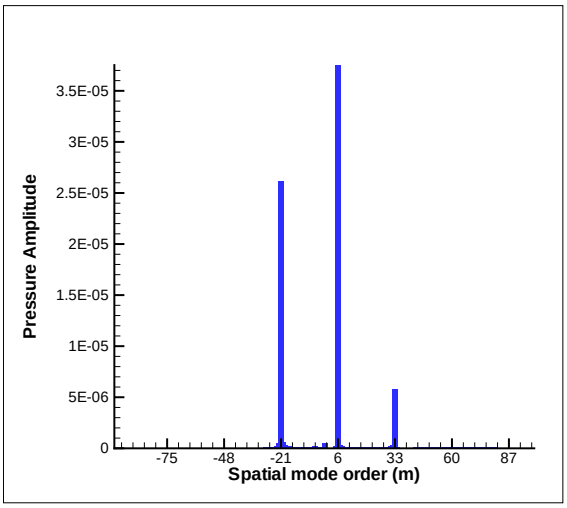

(c) 3BPF

FIG. 7 Modal content of the pressure.

Inflow					
		Upstream going		Downstream going	
n	m	Wavenumber	Wavelength	Wavenumber	Wavelength
2	-5	7.75	0.81	-3.50	-1.79
3	6	9.82	0.64	-4.46	-1.41
3	-21	10.36	0.61	-2.97	-2.11
Outflow					
		Upstream going		Downstream going	
n	m	Wavenumber	Wavelength	Wavenumber	Wavelength
2	-5	6.78	0.93	-3.19	-1.97
3	6	10.36	0.61	-4.97	-1.26
3	-21	4.40	1.43	0.99	6.33

TABLE 3
Wavelengths and wavenumbers of the generated modes.

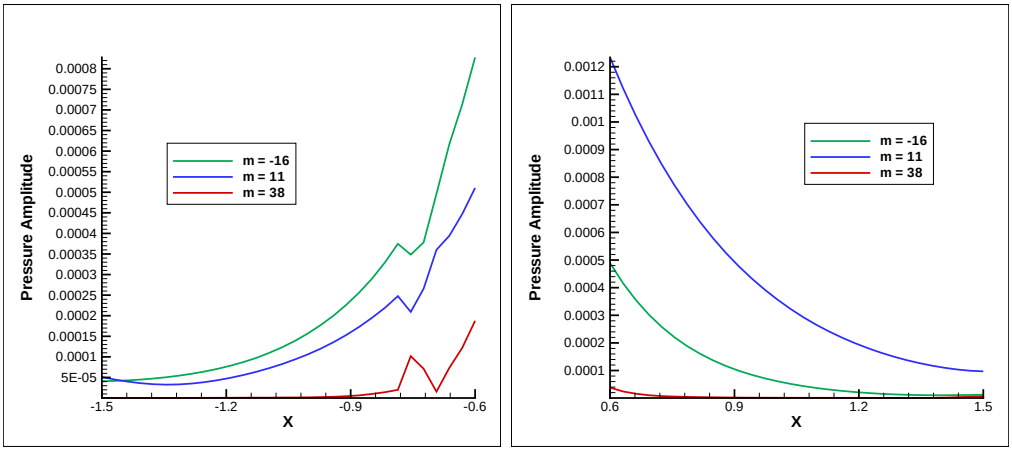

(a) Pressure Amplitude at BPF, inflow.

(b) Pressure Amplitude at BPF, outflow.

FIG. 8: Acoustic waves at BPF (all waves "cut-off").

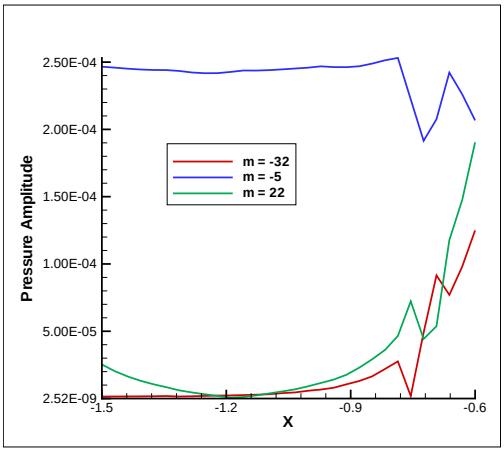

(a) Pressure Amplitude at 2BPF inflow.

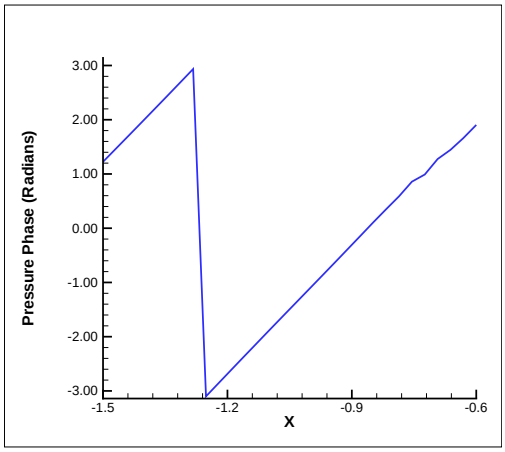

(b) Pressure Phase at 2BPF ($m = -5$) inflow.

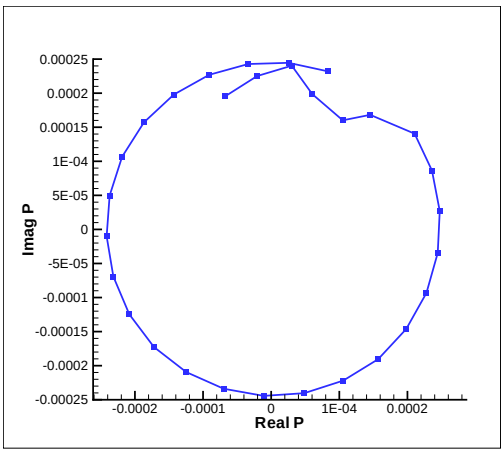

(c) Complex Pressure Amplitude at 2BPF ($m = -5$) inflow.

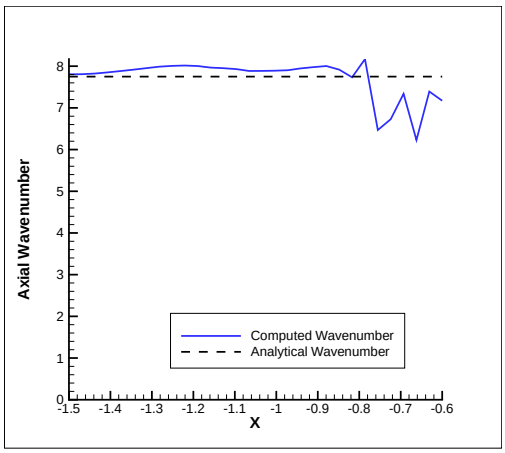

(d) Axial wavenumber for $m = -5$ at 2BPF inflow.

FIG. 9: Acoustic waves at 2BPF ($m = -5$ propagating).

	Relative Flow Angle	Absolute Flow Angle
High loading	45	42.6
Design	50	36
Low loading	55	26.11

TABLE 4
Relative and absolute flow angles at the inflow plane.

The 2BPF acoustic response downstream of the cascade is shown in Fig. 10. The propagating wave $m = -5$ shows signs of a reflection from the downstream boundary, Fig. 10(a). The amplitude of the downstream going wave is $(2.57E-04, 121.3$ dB), and the reflection is approximately 6% of the incident wave. The complex amplitude of the wave, Fig. 10(c), shows a noncircular shape with irregular angular phase difference from point to point. The modulation in amplitude and irregular phase shift are characteristics of an acoustic field with a reflected wave superimposed on the downstream going incident wave. The variation in the point-to-point phase difference is also manifest in the variation of wavenumber, Fig. 10(d).

At 3BPF, there are two modes $m = -21$ and 6 propagating upstream at the inflow, Fig. 11. Again as in the 2BPF response, there is little evidence of reflection from the inflow boundary. The wave amplitudes are nearly constant. The amplitude of the $m = 6$ mode $(3.63E-05, 104.7$ dB) is higher than the amplitude of the $m = -21$ mode $(2.62E-05, 101.9$ dB).

The behavior of the generated modes downstream of the cascade for 3BPF is shown in Fig. 12. The large amplitude of the $m = -21$ mode is evidence of its near resonance condition, Fig. 12(a). Evidence of reflection of the propagating mode $m = 6$ is also seen. The amplitude of the incident wave is $(1.99E-05, 99.5$ dB) with a reflected wave amplitude of approximately 5%.

In summary, the amplitudes of the upstream and downstream propagating waves generated by the rotor-stator interaction are shown in Fig. 13(a) and Fig. 13(b), respectively. In the upstream duct, the waves propagate with little apparent reflection from the inflow boundary. However in the downstream duct, reflections are apparent at the outflow boundary.

7.2. Influence of Steady Vane Loading on Discrete Frequency Noise Generation

The objective of the present research is to determine the impact of steady loading on the acoustic response of a rotor-stator interaction. The response at the design condition was compared with linear theory analysis to verify the generation and propagation characteristics of the acoustic waves[12]. The influence of the steady stator loading on the generated noise is to be accomplished through a series of calculations where the frequency, exit static to stagnation pressure ratio, the mass flow rate, and the rotor wheel speed are maintained relative to the benchmark cascade operating at its design point.

The stator vane is designed for an absolute flow angle $\alpha = 36^\circ$ at the inflow plane with a relative flow angle $\beta = 50^\circ$ specified by the vortical wake. The interest here is to push these flow angles as far as possible from the design condition and determine the influence on the generated noise. Given a relative flow angle, the absolute flow angle can be determined assuming the mass flow rate, the exit static pressure and the rotor wheel speed remain constant, Table 4.

Steady Mach contours are shown in Fig. 14 for the low, design and high loading operating conditions. Interesting results are obtained where the relative flow angle $\beta = 45^\circ$ and the absolute flow angle $\alpha = 42.6^\circ$. Under these conditions, the flow is transonic in the passage. On the suction surface, there is a small region of supersonic flow terminated by a small shock wave.

Fig. 15 shows the steady stator loading and the steady surface Mach number distribution. Two things are apparent. First, the shock on the suction surface is clearly visible for the high loading operating condition ($\beta = 45^o$, $\alpha = 42.6^o$). Second, the reducing absolute flow angle to ($\beta = 55^o$, $\alpha = 26.1^o$) reduces the steady loading significantly.

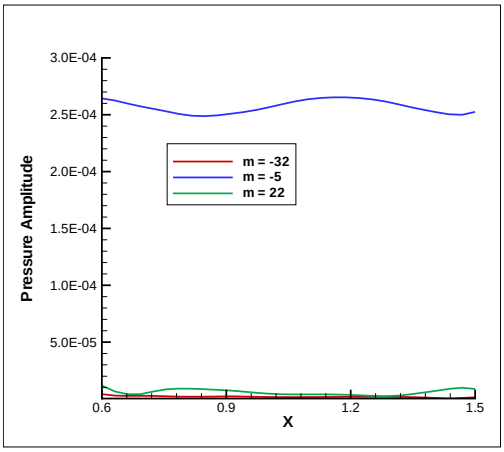

(a) Pressure Amplitude at 2BPF.

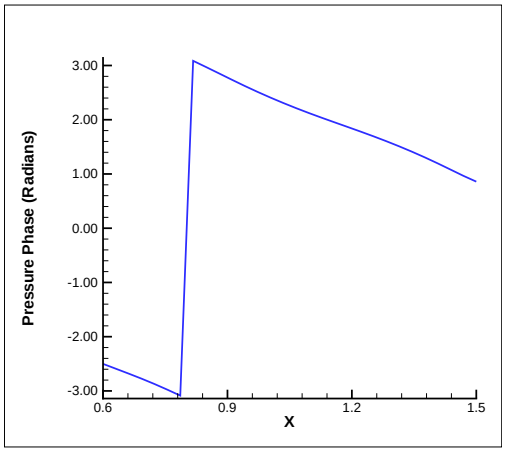

(b) Pressure Phase at 2BPF ($m = -5$).

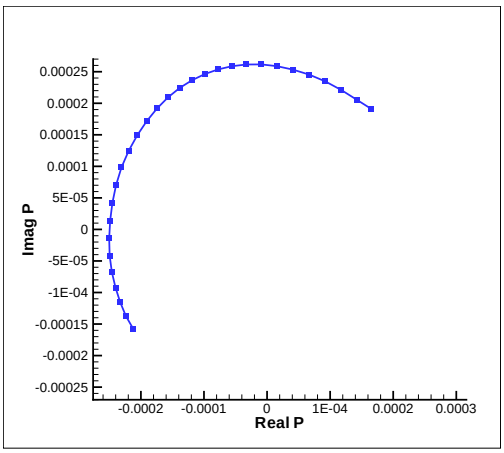

(c) Complex Pressure Amplitude at 2BPF ($m = -5$).

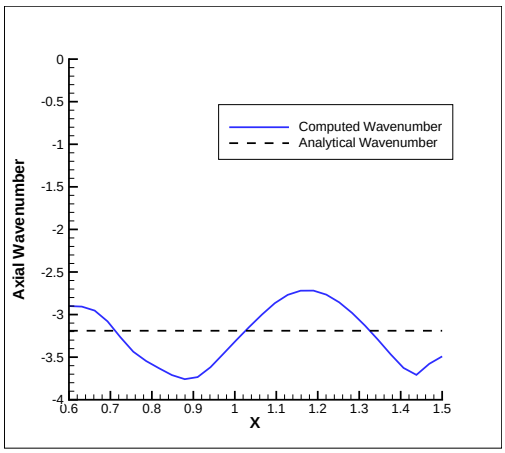

(d) Axial wavenumber for $m = -5$ at 2BPF.

FIG. 10: Acoustic waves downstream at 2BPF ($m = -5$ propagating).

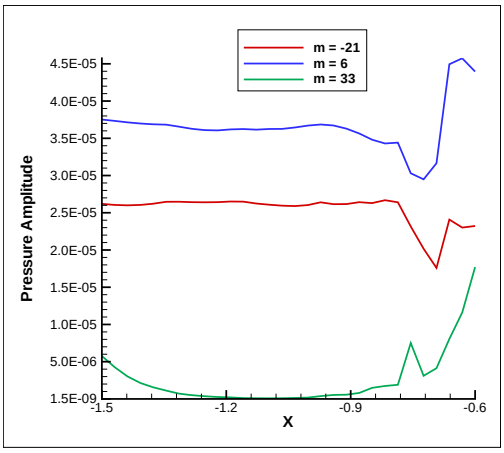

(a) Pressure Amplitude at 3BPF inflow.

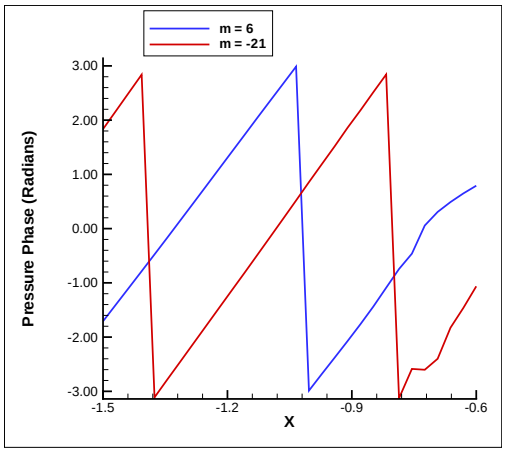

(b) Pressure Phase for propagating modes at 3BPF inflow.

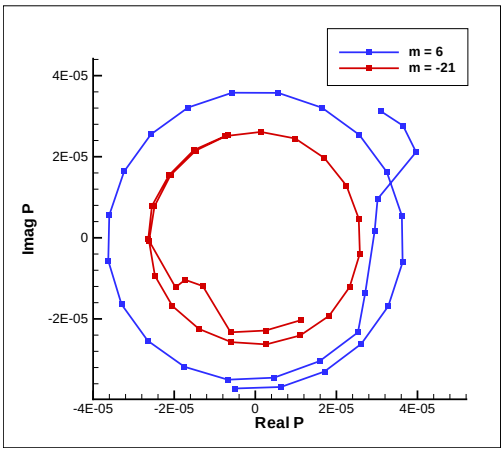

(c) Complex Pressure Amplitude for propagating modes at 3BPF inflow.

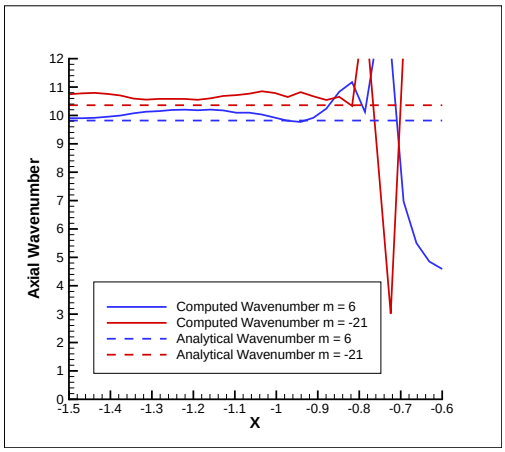

(d) Axial wavenumber for propagating modes at 3BPF inflow.

FIG. 11: Acoustic waves at 3BPF ($m = -21$ and 6 propagating) inflow.

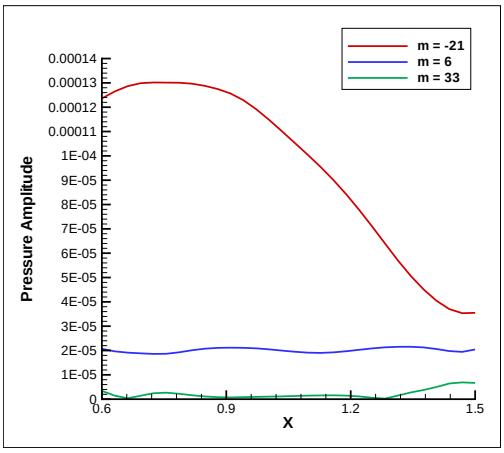

(a) Pressure Amplitude at 3BPF outflow.

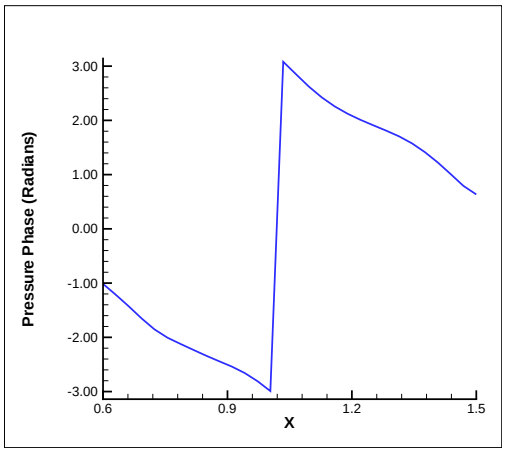

(b) Pressure Phase for $m = 6$ at 3BPF outflow.

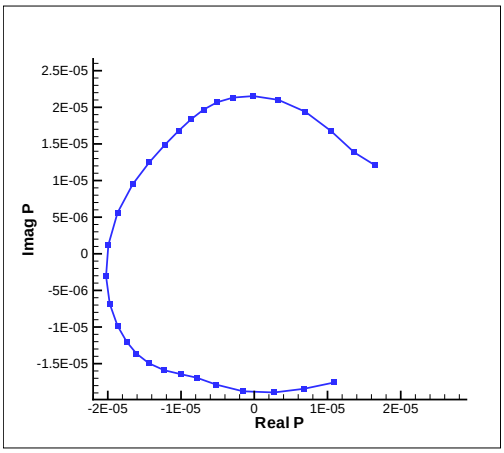

(c) Complex Pressure Amplitude for $m = 6$ at 3BPF outflow.

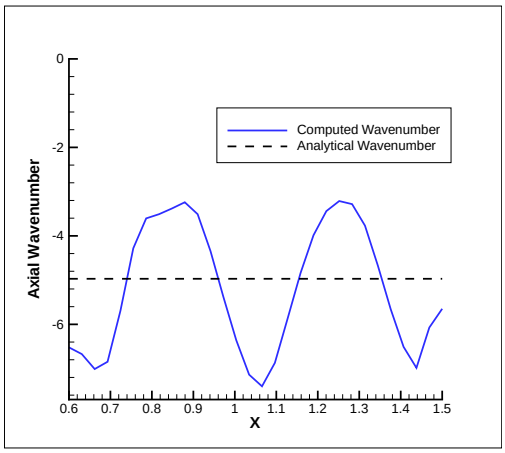

(d) Axial wavenumber for $m = 6$ at 3BPF outflow.

FIG. 12: Acoustic waves at 3BPF ($m = 6$ propagating).

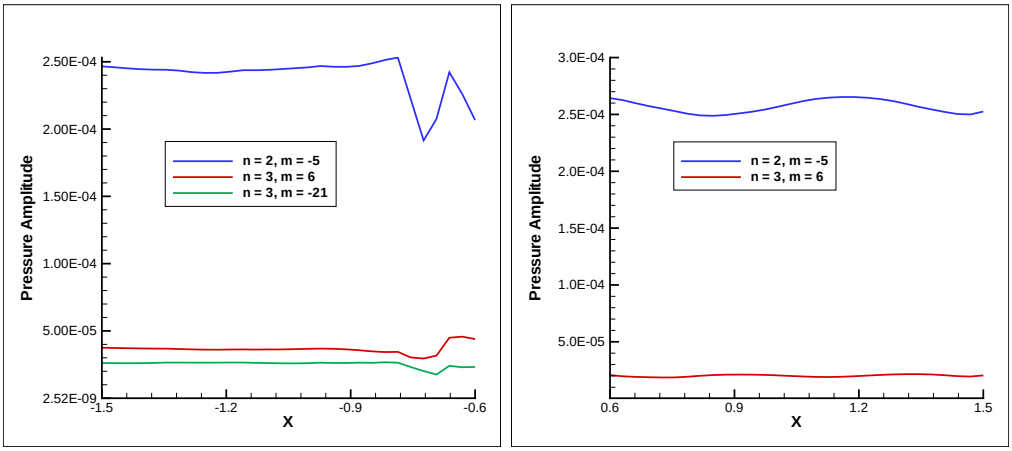

(a) inflow duct

(b) outflow duct

FIG. 13: Propagating acoustic waves generated in the exit duct.

The response to the convected vortical gust is decomposed as a function of frequency and spatial mode order. With $N_R = 11$ rotor blades and $N_S = 27$ stator vanes, the stator is cut-off at BPF and produces no propagating acoustic waves. At 2BPF, one acoustic wave $m = -5$ propagates. At 3BPF however, two acoustic waves propagate $m = -21$ and 6 in the inlet due to the swirl, but only one $m = 6$ propagates in the axial flow downstream of the stator.

The influence of steady loading on the propagating acoustic wave at 2BPF is shown in Fig. 16. Upstream of the stator, the increasing the loading has a significant effect. The amplitude of the wave increases by more than 150% from the design condition. Decreasing the loading has a smaller effect the amplitude of the wave is reduced by only 30% from the design condition. Downstream of the stator, decreasing the loading has very little effect on the generated noise. However, increasing the loading increases the downstream acoustic response by nearly 50%.

At 3BPF, the acoustic response is complicated by the swirling flow between the rotor and stator. The rotor-stator interaction generates modes satisfy $m = ..., \ -21, \ 6, ...$ The lowest order mode $m = 6$ propagates upstream and downstream. However, the swirl ($\alpha = 26.1^o, \ 36^o$ and 42.6^o) in the low, design and high loading operating conditions, respectively, causes an additional acoustic wave $m = -21$ to propagate upstream. The amplitude of the propagating acoustic waves upstream and downstream of the stator are shown in Fig. 17. Once again, increasing the loading has the greatest impact on the upstream propagating waves. The amplitude of the $m = -21$ and 6 waves increase by 280% and 150%, respectively. Smaller variations on the order of 25% are seen with a decrease in loading. Downstream of the stator, increasing the stator loading has a similar dramatic impact on the generated noise. The amplitude of the propagating wave $m = 6$ increases by nearly 150%.

Finally, these results can best be summarized by examining the change in amplitude in decibels, Fig. 18. The highly loaded stator shows and increase of roughly 10 dB upstream and 5-10 dB downstream. Reducing the stator load had a much less dramatic effect with noise reduction on the order of 1-5 dB.

8. ACKNOWLEDGMENTS

The Principal Investigator is thankful for the technical correspondence and support of the NASA Glenn CAA team, Dr. Ray Hixon, Dr. Nals Nallasamy, Dr. Rodger Dyson and Dr. Ed Envia. The Principal Inves-

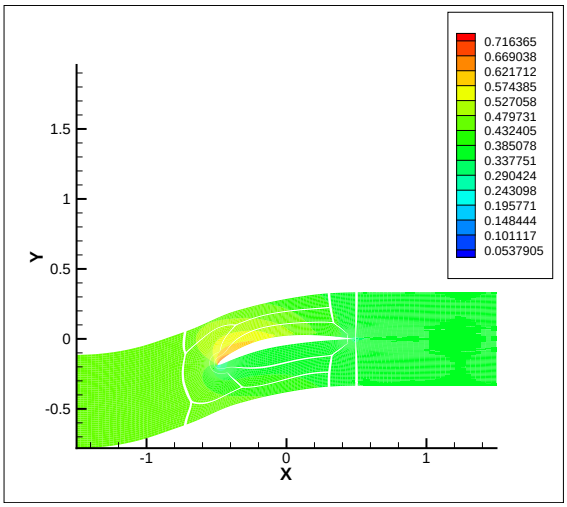

(a) Steady Mach contours design condition ($\beta = 50^o, \alpha = 36^o$).

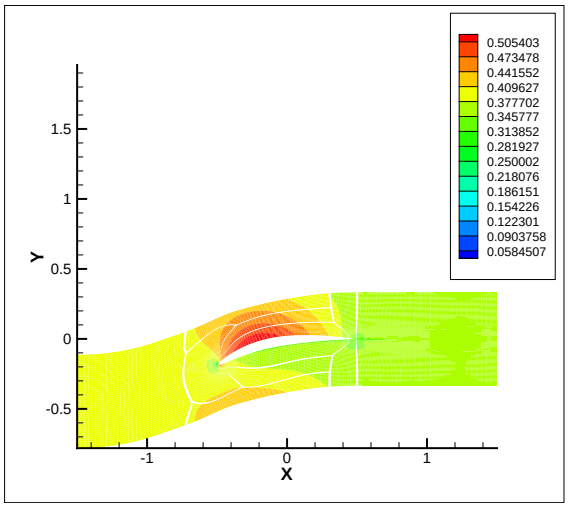

(b) Steady Mach contours low loading condition ($\beta = 55^o, \alpha = 26.1^o$).

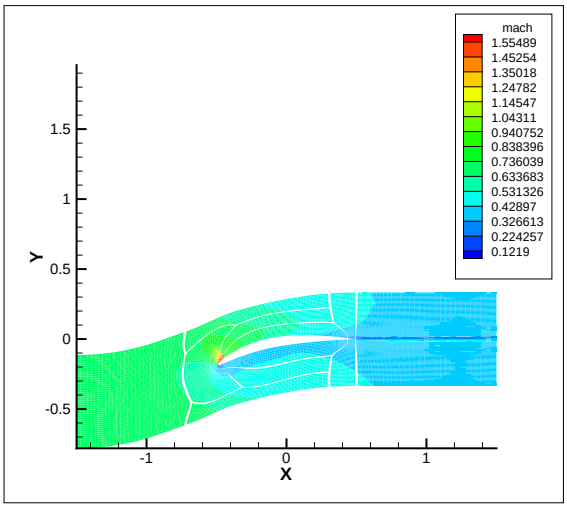

(c) Steady Mach contours high loading condition ($\beta = 45^o, \alpha = 42.6^o$).

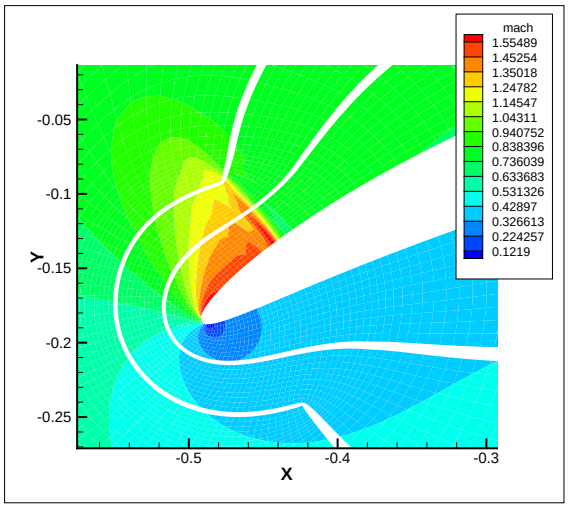

(d) Steady Mach contours high loading condition - leading edge ($\beta = 45^o, \alpha = 42.6^o$).

FIG. 14: Steady Mach numbers over the stator passage.

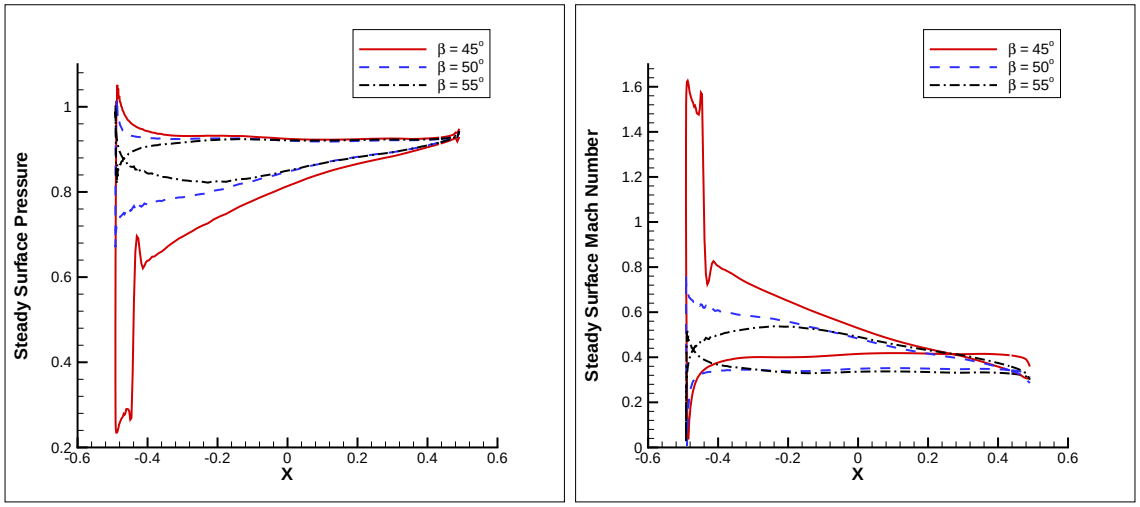

(a) Steady stator loading.

(b) Steady surface Mach numbers.

FIG. 15: Steady stator loading and surface Mach numbers.

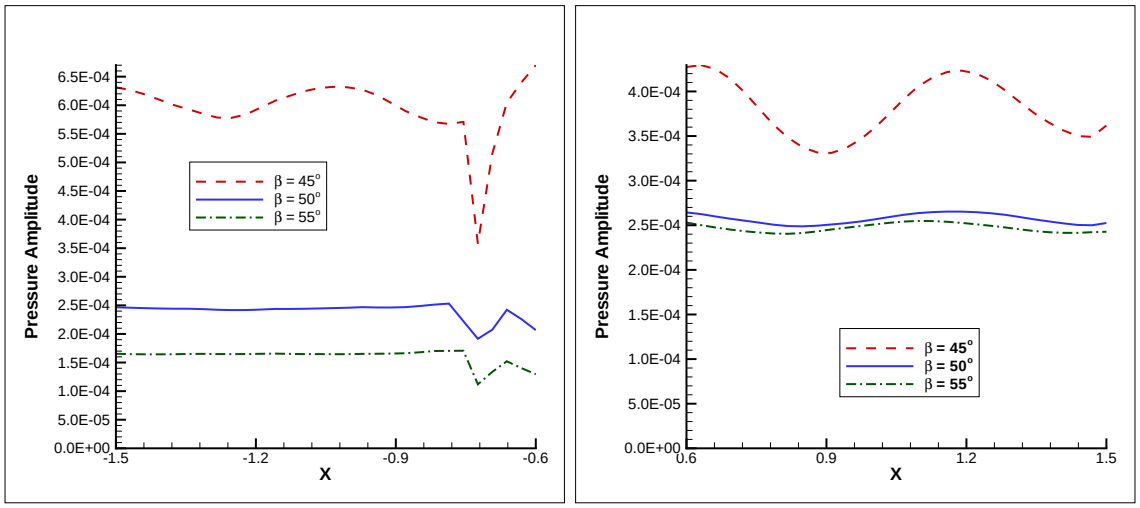

(a) Upstream of stator vane.

(b) Downstream of stator .

FIG. 16: 2BPF acoustic response $m = -5$ propagating.

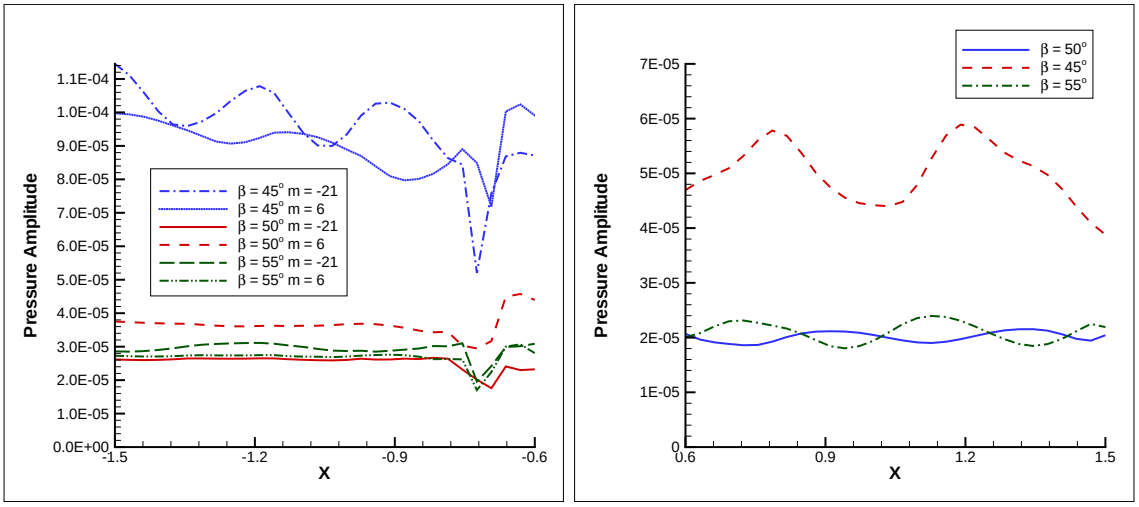

(a) Upstream of stator vane.

(b) Downstream of stator .

FIG. 17: 2BPF acoustic response $m = 6$ propagating.

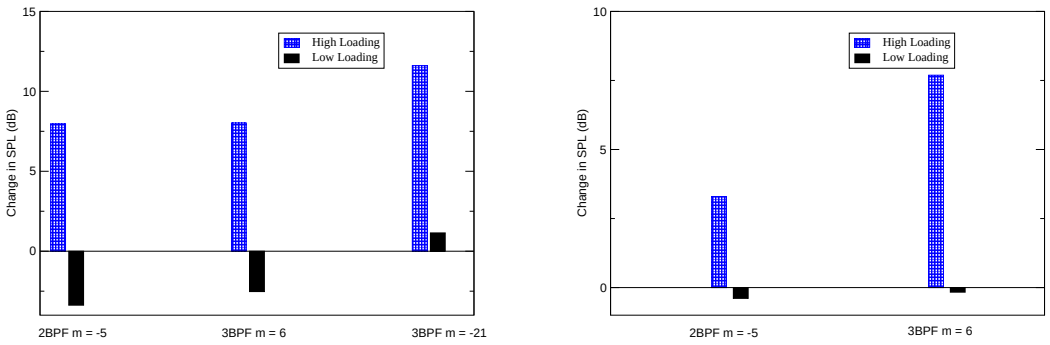

(a) Upstream response.

(b) Downstream response.

FIG. 18: Two-dimensional cascade representation.

tigator would also like to recognize Dr. Christopher Miller who was responsible for the setup, maintenance and administration of the Beowulf cluster used for these computations.

REFERENCES

[1] K.C. Hall and W. Clark, "Linearized Euler Predictions of Unsteady Aerodynamic Loads in Cascades," AIAA Journal, Vol. 31, pp. 540-550.

[2] K.C. Hall and J.M. Verdon, "Gust Response Analysis for Cascades Operating in Nonuniform Mean Flows," AIAA Journal, Vol. 29, pp. 1463-1471.

[3] D. Prasad and J.M. Verdon, "A Three-Dimensional Linearized Euler Analysis of Classical Wake/Stator Interactions: Validation and Unsteady Response Predictions," International Journal of Aeroacoustics, Vol. 1, No. 2, 2002, pp. 137-163.

[4] R. Hixon, R. R. Mankbadi and J. R. Scott, "Validation of High-Order Prefactored Compact Code on Nonlinear flows with Complex Geometries", AIAA Paper 2001-1103, Reno, NV, January 2001.

[5] D.P. Lockard and P.J. Morris, "Radiated Noise from Airfoils in Realistic Mean Flow," AIAA Journal, Vol. 36, pp. 907-914.

[6] D.P. Lockard and P.J. Morris, "A Parallel Implementation of a Computational Aeroacoustic Algorithm for Airfoil Noise," AIAA Paper 96-1754, 1976.

[7] J.M. Tyler and T.G. Sofrin, "Axial Flow Compressor Noise Studies," SAE Transactions, Vol. 70, 1962, pp. 309-322.

[8] R. Hixon, "A New Class of Compact Schemes", AIAA Paper 98-0367, Reno, NV, January 1998.

[9] F. Q. Hu, M. Y. Hussaini, and J. L. Manthey, "Low-Dissipation and Low-Dispersion Runge-Kutta Schemes for Computational Acoustics", J Comp. Phys., Vol. 124, No. 1, 1996, pp. 177-191.

[10] M. D. Giles, "Non-reflecting Boundary Conditions for Euler Equations Calculations", AIAA Journal, No. 28, 1990, pp. 2050-2058.

[11] S. N. Smith, "Discrete Frequency Sound Generation in Axial Flow Turbomachines," Aeronautical Research Council Reports and Memoranda, No. 3709, 1973.

[12] S. Sawyer, M. Nallasamy, R. Hixon and R. Dyson, "Computational Aeroacoustic Prediction of Discrete Frequency Noise Generated by a Rotor-Stator Interaction", International Journal of Aeroacoustics, 1 January 2004, Vol. 3, No. 1, pp. 67-86.

[13] S. Sawyer, M. Nallasamy, R. Hixon, and R. Dyson, "The Influence of Steady Loading on Discrete-Frequency Rotor-Stator Interaction Noise", AIAA Paper 2003-4419, Huntsville, AL, July 2003.